Monthly Notices of the ROYAL ASTRONOMICAL SOCIETY

MNRAS **524,** 5050–5059 (2023) https://doi.org/10.1093/mnras/stad2190
Advance Access publication 2023 July 21

AMICO galaxy clusters in KiDS-DR3: Constraints on ΛCDM from extreme value statistics

V. Busillo [1,2,3★] G. Covone [1,2,3] M. Sereno [4,5] L. Ingoglia [4] M. Radovich [6] S. Bardelli,[5] G. Castignani,[4,5] C. Giocoli [4,5,7] G. F. Lesci [4,5] F. Marulli [4,5,7] M. Maturi,[8,9] L. Moscardini [4,5,7] E. Puddu[2] and M. Roncarelli [5]

[1]*Dipartimento di Fisica 'E. Pancini', Università di Napoli Federico II, C.U. di Monte Sant'Angelo, via Cintia, I-80126 Napoli, Italy*
[2]*INAF, Osservatorio Astronomico di Capodimonte, Salita Moiariello 16, I-80131, Napoli, Italy*
[3]*INFN, Sez. di Napoli, Compl. Univ. Monte S. Angelo, Via Cinthia, I-80126 Napoli, Italy*
[4]*Dipartimento di Fisica e Astronomia 'Augusto Righi' - Alma Mater Studiorum Università di Bologna, via Piero Gobetti 93/2, I-40129 Bologna, Italy*
[5]*INAF, Osservatorio di Astrofisica e Scienza dello Spazio di Bologna, via Piero Gobetti 93/3, I-40129 Bologna, Italy*
[6]*INAF, Osservatorio Astronomico di Padova, vicolo dell'Osservatorio 5, I-35122 Padova, Italy*
[7]*INFN, Sezione di Bologna, viale Berti Pichat 6/2, I-40127 Bologna, Italy*
[8]*Zentrum für Astronomie, Universität Heidelberg, Philosophenweg 12, D-69120 Heidelberg, Germany*
[9]*ITP, Universität Heidelberg, Philosophenweg 16, D-69120 Heidelberg, Germany*

Accepted 2023 July 18. Received 2023 June 19; in original form 2023 March 7

ABSTRACT

We constrain the ΛCDM cosmological parameter σ_8 by applying the extreme value statistics for galaxy cluster mass on the AMICO KiDS-DR3 catalogue. We sample the posterior distribution of the parameters by considering the likelihood of observing the largest cluster mass value in a sample of $N_{\rm obs} = 3644$ clusters with intrinsic richness $\lambda^* > 20$ in the redshift range $z \in [0.10, 0.60]$. We obtain $\sigma_8 = 0.90^{+0.20}_{-0.18}$, consistent within 1σ with the measurements obtained by the Planck collaboration and with previous results from cluster cosmology exploiting AMICO KiDS-DR3. The constraints could improve by applying this method to forthcoming missions, such as *Euclid* and LSST, which are expected to deliver thousands of distant and massive clusters.

Key words: gravitational lensing: weak – cosmological parameters – large-scale structure of Universe – cosmology: theory.

1 INTRODUCTION

The extreme value statistics (EVS; Gumbel 1958) seeks to determine how likely the highest valued observations of a random variable is. In the last decades, this theory has seen various applications in astrophysics and cosmology. For instance, it has been used to analyse the luminosity distribution of the most massive galaxies in a galaxy cluster (Bhavsar & Barrow 1985), the convective penetration in radiative-convective boundaries of pre-main sequence stars (Pratt et al. 2017), and the most massive haloes in the Universe (Sheth & Diaferio 2011; Waizmann, Ettori & Moscardini 2011; Holz & Perlmutter 2012; Waizmann, Ettori & Moscardini 2012). In particular, it has been used to predict the probability distribution for the most massive galaxy cluster in a given region of the Universe, with results that are highly consistent with predictions from large well resolved cosmological *N*-body simulations (Davis et al. 2011).

In cosmology, this approach has been used to verify whether the observation of rare astrophysical objects is compatible with the predictions from a cosmological model (for example, the Λ-cold dark matter standard cosmological model, ΛCDM). Harrison & Coles (2011) applied the EVS to galaxy clusters to check if the most massive galaxy clusters were in agreement with the standard cosmological model or with alternative models that predict an enhanced structure formation, with all the clusters considered showing concordance with a ΛCDM cosmology. Kim et al. (2021) used the same approach as a rarity test to check whether the physical properties of the galaxy cluster ACT-CL J0102–4915 (also known as 'El Gordo') were compatible with the ΛCDM paradigm, finding its mass compatible with ΛCDM predictions within 2σ.

More recently, Lovell et al. (2022) applied the EVS to Hubble Space Telescope and *JWST* observations of high-redshift galaxies, to verify whether these objects were in tension with the standard cosmological model. They found significant tension with ΛCDM predictions for some $z \gtrsim 10$ galaxies taken from the recent *JWST* high-redshift candidates.

An approach using the EVS with respect to cosmological parameters was also studied in Reischke, Maturi & Bartelmann (2016), where the asymptotic limit of the EVS distribution for a large number of observations, the generalized extreme value distribution, has been applied to mock weak lensing shear peak counts from an *Euclid*-like survey to find confidence regions for the amplitude of the linear matter density fluctuations σ_8, the matter density parameter, $\Omega_{\rm m}$, and the dark energy equation of state parameter, w_0.

The inferred values of $S_8 \equiv \sigma_8\sqrt{\Omega_{\rm m}/0.3}$ indicate a discrepancy, as demonstrated in Douspis, Salvati & Aghanim (2019) and Corasaniti, Sereno & Ettori (2021), between late-time studies, such as cosmic shear measurements (Hikage et al. 2019; Asgari et al. 2021) and early-epoch investigations, for example those derived from primary CMB analysis (Planck Collaboration I 2014, 2020a). This tension

★ E-mail: valerio.busillo@inaf.it

is significant at a 2σ–4σ level (refer to Abdalla et al. 2022 for a review). Consequently, it is crucial to examine how findings based primarily on cluster mass measurements compare to this tension.

Here, we apply EVS to the highest value of galaxy cluster mass in a survey, to constrain the value of σ_8. We consider the cluster catalogue presented in Maturi et al. (2019), which was built by using the adaptive matched identifier of clustered objects (AMICO) algorithm (Bellagamba et al. 2018) on the third data release of the Kilo-Degree Survey (KiDS-DR3, de Jong et al. 2017).

The paper is organized as follows: In Section 2 we briefly present the AMICO KiDS-DR3 cluster catalogue. In Section 3, we construct the probability distribution for the mass of the most massive cluster expected in the catalogue. In Section 4, we describe the likelihood on which we perform the Bayesian inference of the relevant cosmological parameters and compare the observations from the AMICO KiDS-DR3 catalogue to the theoretical predictions. The results of the analysis are presented in Section 5, and are discussed in Section 6. Section 7 is dedicated to the analysis of systematics, such as the uncertainty due to the mass function model and the uncertainty related to the mass ranking. Lastly, our conclusions are presented in Section 8.

All the cluster masses considered in this work are defined using M_{200c}, i.e. the mass inside a sphere that encloses an average mass density equal to 200 times the critical density of the Universe at the cluster redshift.[1] We also define $\log_{10}[M_{200c}\,(10^{14}\,h^{-1}\,\mathrm{M}_\odot)] = \mu$, for brevity. In this work, we assume a flat ΛCDM cosmology with only two free parameters, σ_8 and Ω_m. All the other parameters, for example the dark energy density parameter, Ω_Λ, the dark energy equation-of-state parameter, w, the Hubble constant, H_0, and the spectral index, n_s, are fixed to the values estimated in Planck Collaboration VI (2020b), table 2 (TT, TE, and EE+lowE). All the results shown in this work are given in terms of 16th, 50th (median), and 84th percentiles of the respective distributions.

2 THE AMICO KIDS-DR3 CLUSTER CATALOGUE

The clusters used in this work were detected in the third data release (DR3) of KiDS (de Jong et al. 2013; Kuijken et al. 2015; de Jong et al. 2017). KiDS is a European Southern Observatory (ESO) wide-field imaging survey made with the OmegaCAM camera (Kuijken 2011) mounted on the Very Large Telescope (VLT)/ Survey Telescope (VST; Capaccioli & Schipani 2011), designed to observe in the (u, g, r, i) bands an area of 1350 deg^2, down to the limiting magnitudes of 24.3, 25.1, 24.9, and 23.8 for each of the bands, respectively. The DR3 covers an area of 438 deg^2 (377 deg^2 after removing areas affected by artefacts such as reflection haloes around bright stars and satellite tracks; see de Jong et al. 2015; Kuijken et al. 2015).

Maturi et al. (2019) presented a catalogue of clusters found in KiDS-DR3 with AMICO, a code designed for the detection of galaxy clusters in photometric surveys, first tested on mock photometric galaxy catalogues derived in Bellagamba et al. (2018). The detection algorithm is based on the Optimal Filtering technique (Maturi et al. 2005; Bellagamba et al. 2011; Radovich et al. 2017). As detailed in Maturi et al. (2019), AMICO models the data as the sum of a signal term and a noise term, and uses an iterative method to evaluate the signal amplitude by filtering the raw data with a filter evaluated on a 3D grid ($\boldsymbol{\theta}_c, z_c$), where $\boldsymbol{\theta}_c$ is the sky coordinate vector, given in terms of right ascension and declination, and z_c is the redshift (Bellagamba et al. 2018). As grid resolution, Maturi et al. (2019) considered 0.3 arcmin for each of the $\boldsymbol{\theta}_c$ components and 0.01 for the redshift.

A cluster is localized by considering the location in the 'sky coordinates-redshift' space ($\boldsymbol{\theta}_c, z_c$) which maximizes the amplitude $A(\boldsymbol{\theta}_c, z_c)$. The model used to describe the signal term is the product of a Schechter luminosity function (Schechter 1976) by a Navarro–Frenk–White radial density profile (Navarro, Frenk & White 1997). Once a detection is defined, AMICO also assigns to each galaxy a membership probability to belong to the j-th cluster, based on the value of the amplitude signal A and on the observed properties (sky position, photometric redshift distribution and magnitude) of the galaxy.

It should be noted that, as described in Bellagamba et al. (2018), AMICO can be considered a 3D detection algorithm, since it considers the photometric redshift distribution of each galaxy when computing the amplitude and S/N of each detection. In particular, a cleaning procedure was applied, which was specifically designed to minimize blending and projection effects.

Among the different mass proxies provided by AMICO, in this work we used the intrinsic richness λ^* as the mass proxy, defined as:

$$\lambda^*_j = \sum_{i=1}^{N_\mathrm{gal}} P_i(j) \quad \text{with} \quad \begin{cases} m_i < m^*(z_j) + 1.5 \\ R_i(j) < R_\mathrm{max}(z_j) \end{cases} , \tag{1}$$

where $P_i(j)$ is the membership probability for the j-th cluster located at redshift z_j, m_i is the magnitude of the galaxy, m^* the Schechter function reference magnitude, R_i is the distance of the galaxy from the centre of the cluster and R_max is the radius of a sphere enclosing a mass $M_{200c} = 10^{14}\,h^{-1}\,\mathrm{M}_\odot$. This choice is made because the intrinsic richness is a reliable halo mass proxy, which is fundamental for cosmological studies using clusters.

The mass-richness relation used to convert the mass proxy is:

$$\mu_\chi(z;\lambda^*) = \alpha + \beta \log_{10}\left(\frac{\lambda^*}{\lambda^*_\mathrm{piv}}\right) + \gamma \log_{10}\left(\frac{E(z)}{E(z_\mathrm{piv})}\right) , \tag{2}$$

where $\alpha = 0.004 \pm 0.038$, $\beta = 1.71 \pm 0.08$, $\gamma = -1.33 \pm 0.64$, $\lambda^*_\mathrm{piv} = 30$, and $z_\mathrm{piv} = 0.35$. The scatter of this relation is given by $\log_{10}(\sigma_{\mu|\lambda^*}) = -1.13 \pm 0.53$ (Sereno et al. 2020). The relation was calibrated with weak lensing mass estimates in Bellagamba et al. (2019), which we refer to for details.

The AMICO KiDS-DR3 catalogue (Maturi et al. 2019) contains 7988 clusters, down to $S/N = 3.5$, in the redshift range $z \in [0.10, 0.80]$. For the analysis, we used the cluster redshifts corrected for the bias discussed in Maturi et al. (2019), and we ranked the cluster masses M_{200c} based on the respective intrinsic richness λ^*.

To be consistent with the scaling relation parameter estimates obtained in Bellagamba et al. (2019), we restricted ourselves to the redshift interval $z \in [0.10, 0.60]$ and filtered out all the clusters with intrinsic richness $\lambda^* \leq 20$, leaving $N_\mathrm{obs} = 3644$ clusters. This ensures a purity of the sample of more than 98 per cent over the whole interval, and a completeness of ∼84 per cent in the redshift range $z \in [0.10, 0.30]$, ∼79 per cent in the range $z \in [0.30, 0.45]$, and ∼58 per cent in the range $z \in [0.45, 0.60]$ (see Maturi et al. 2019, fig. 12). Fig. 1 shows the redshift and mass distributions of the galaxy clusters in our sample.

The most massive cluster in AMICO KiDS-DR3 is AK3 J091606.48-002328, also known as Abell 776. This cluster is located at redshift $z = 0.37$, and has an intrinsic richness of $\lambda^* = 137 \pm 24$, with a corresponding mass of $M_{200c} = (13.3 \pm 4.9) \times 10^{14}\,h^{-1}\,\mathrm{M}_\odot$. The corresponding log-mass is $\mu = 1.12 \pm 0.16$. This cluster is also

[1] $\rho_c(z) = 3H(z)^2/8\pi G$

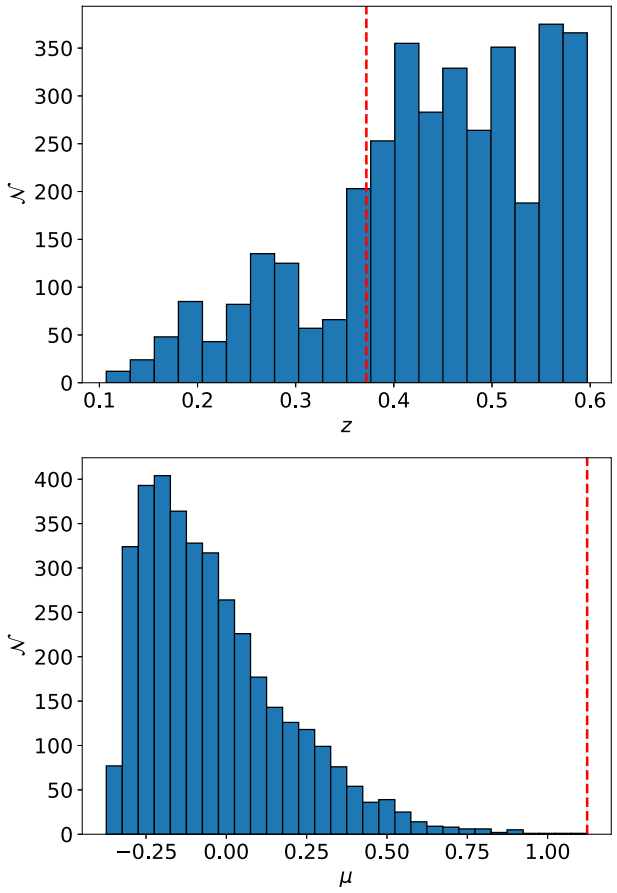

Figure 1. Redshift and mass distributions of the clusters in the AMICO KiDS-DR3 catalogue having $\lambda^* > 20$ and z in the redshift range [0.10, 0.60]. *Top panel*: redshift distribution. *Bottom panel*: mass distribution. The dashed vertical red lines represent the redshift and mass associated with the most massive cluster of the catalogue.

Table 1. Mass estimates of Abell 776, along with the measurement method used to determine them.

M_{200c} $[10^{14}\,h^{-1}\,\mathrm{M}_\odot]$	Method	Reference
13.3 ± 4.9	Richness	This work
$5.61^{+1.96}_{-1.68}$	Weak Lensing	Hamana, Shirasaki & Lin (2020)
$8.10^{+3.26}_{-2.17}$	Weak Lensing	Medezinski et al. (2018)
$4.33^{+0.58}_{-0.56}$	Sunyaev-Zel'dovich	Planck Collaboration XXVII (2016)

present in Hamana et al. (2020) and Medezinski et al. (2018), with masses reported in Table 1. Fig. 2 shows an image of Abell 776.

As detailed in Sereno (2015), weak lensing mass estimates depend on the cosmological parameters via the equation:

$$M_\Delta^{\mathrm{WL}} \propto D_\mathrm{d}^{-3\delta_\gamma/(2-\delta_\gamma)} \left(\frac{D_\mathrm{ds}}{D_\mathrm{s}}\right)^{-3/(2-\delta_\gamma)} \times [H(z)]^{-(1+\delta_\gamma)/(1-\delta_\gamma/2)}\,, \tag{3}$$

where z is the redshift of the cluster, δ_γ is a parameter related to the slope of the angular mass profile, D_d is the observer-lens angular-diameter distance, D_s is the observer-source angular-diameter distance and D_ds is the lens-source angular-diameter distance. Therefore, when changing the underlying cosmology, one should correct

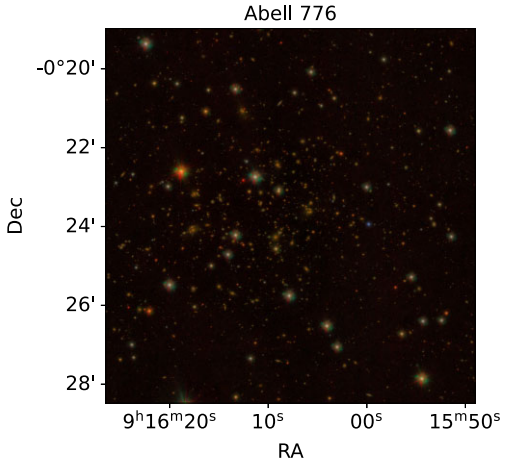

Figure 2. Colour composite (g, r, i) image relative to J091606.48-002328, also known as Abell 776. The stamp shows a $\approx 6' \times 6'$ region centred on the location identified by the AMICO algorithm.

the observed mass value via the formula:

$$M_{\Delta,\mathrm{new}} = \frac{\alpha_\mathrm{new}}{\alpha_\mathrm{old}} M_{\Delta,\mathrm{old}}\,, \tag{4}$$

where α_new is the factor defined in equation (3), evaluated with the new choice of cosmological parameters, while α_old is the same factor, but evaluated assuming the reference cosmology.

3 EVS FOR CLUSTER MASSES

The probability distribution of the largest cluster mass, M_max, in a sample $\{M_i\}$ of N clusters, i.e. the maximum mass $M_\mathrm{max} = \max(M_i)$, was discussed e.g. in Harrison & Coles (2011) and Waizmann, Ettori & Bartelmann (2013).

If all the M_i values are drawn from the same probability distribution, and the measurements are independent, the probability density function $\phi : \mathrm{d}P(M_\mathrm{max} = M|N) = \phi(M)\,\mathrm{d}M$ associated to the highest order statistics in mass is given by (Waizmann et al. 2013, appendix A1):

$$\phi(M_\mathrm{max} = M; N) = N\, f(M)\, [F(M)]^{N-1}\,, \tag{5}$$

while the associated cumulative distribution function is:

$$\Phi(M_\mathrm{max} \leq M; N) = \int_0^M \phi(m)\, dm = [F(M)]^N. \tag{6}$$

The distributions $f(M)$ and $F(M)$ are the probability density function and the cumulative distribution function of a galaxy cluster of mass M in a region of the sky, respectively. These distributions can be written in terms of the halo mass function, $\mathrm{d}n/\mathrm{d}M$, which describes the number density of clusters expected to have a mass between M and $M + \mathrm{d}M$, and the comoving volume per unit of redshift, $\mathrm{d}V/\mathrm{d}z$.

Following Waizmann et al. (2013), these distributions can be written for a fixed redshift range $[z_\mathrm{min},\ z_\mathrm{max}]$ as:

$$f(M) = \frac{f_\mathrm{sky}}{N_\mathrm{tot}} \int_{z_\mathrm{min}}^{z_\mathrm{max}} \chi(M, z; \lambda^*_\mathrm{th})\, \frac{\mathrm{d}n}{\mathrm{d}M}(M, z)\, \frac{\mathrm{d}V}{\mathrm{d}z}(z)\, \mathrm{d}z, \tag{7}$$

$$F(M) = \int_{M_\mathrm{min}}^{M} f(m)\, \mathrm{d}m, \tag{8}$$

where f_sky is the fraction of the sky covered by the survey, and:

$$N_\mathrm{tot} = f_\mathrm{sky} \int_{M_\mathrm{min}}^{M_\mathrm{max}} \int_{z_\mathrm{min}}^{z_\mathrm{max}} \chi(M, z; \lambda^*_\mathrm{th})\, \frac{\mathrm{d}n}{\mathrm{d}M}(M, z)\, \frac{\mathrm{d}V}{\mathrm{d}z}(z)\, \mathrm{d}z\, \mathrm{d}M\,. \tag{9}$$

The function χ that appears in equations (7), (8), and (9) is the selection function, which accounts for the fact that it is not possible to detect all galaxy clusters theoretically observable in a certain Universe volume, due to limited depth or accuracy of the detection algorithm. The parameter $\lambda^*_{\rm th}$ is the threshold in cluster richness, which we fixed to 20 (see Section 2).

The selection function χ can be approximated as (Sereno & Ettori 2015):

$$\chi(\mu, z; \lambda^*_{\rm th}) = \frac{1}{2}\mathrm{erfc}\left(\frac{\mu_\chi(z;\lambda^*_{\rm th}) - \mu}{\sqrt{2}\sigma_\chi}\right), \quad (10)$$

the scale σ_χ can be written in terms of uncertainty on mass estimates, obtained by adding in quadrature the intrinsic scatter of the mass-richness relation to the uncertainty associated to the scaling parameters in equation (2), and the uncertainty associated to the richness, $\delta\lambda^*/\lambda^* \sim 18$ per cent (Maturi et al. 2019).

As a reference, we consider the halo mass function from Despali et al. (2016). In Section 7.1 we will discuss the possible systematics introduced by this choice. We used a single redshift interval for evaluating equations (7)–(9), fixing $z_{\rm min} = 0.10$ and $z_{\rm max} = 0.60$.

4 STATISTICAL MODEL

In the following, we consider a flat ΛCDM cosmological model with only two free parameters, σ_8 and $\Omega_{\rm m}$. The observed quantities are two: the observed log-mass of Abell 776, $\mu_{\rm max,obs}$, and the observed cluster count, $N_{\rm obs}$. The model parameters are four: the ΛCDM cosmological parameters σ_8 and $\Omega_{\rm m}$, the true log-mass of Abell 776, $\mu_{\rm max,true}$, and the true cluster count, $N_{\rm true}$.

The likelihood distribution is the probability of the largest mass estimate in the survey and of the observed number cluster count for a given set of cosmological parameters and the true values of the mass and of the cluster count.

We used the following functional form for the likelihood:

$$L = \mathcal{G}(\mu_{\rm max,\,obs}|\,\mu_{\rm max,\,true},\,\sigma_\mu)\cdot\mathcal{P}(N_{\rm obs}|\,N_{\rm true}) \times\ \phi(\mu_{\rm max,\,true}|\,N_{\rm true},\,\sigma_8,\,\Omega_{\rm m})\,, \quad (11)$$

which is the product of three distributions:

(i) A Gaussian distribution, $\mathcal{G}$, centred on the expected log-mass value $\mu_{\rm max,true}$ and evaluated for $\mu = \mu_{\rm max,obs}$, with a standard deviation equal to the statistical uncertainty on the mass;
(ii) A Poisson distribution, $\mathcal{P}$, with expected value equal to $N_{\rm true}$ and evaluated for $N = N_{\rm obs}$. This term takes into account the probability of observing a cluster count equal to $N_{\rm obs}$;
(iii) The EVS distribution, ϕ, evaluated for $\mu = \mu_{\rm max,true}$, which gives the probability of observing a given log-mass for the most massive cluster, in a region of the sky where $N_{\rm true}$ clusters are located, having a log-mass equal to $\mu_{\rm max,true}$.

We want to remark that our approach is complementary to the one commonly used in cosmological inference from cluster abundance, where the number count is written in terms of the halo mass function and the cosmological parameters (see e.g. Equation 9), in that we instead treat $N_{\rm true}$ as a model parameter to be marginalized over.

Finally, to estimate the full posterior distribution, we considered uniform priors, $\mathcal{U}$, for all the parameters, with bounds reported in Table 2.

Table 2. Parameters associated to the likelihood distribution described in Section 4.

Parameter	Prior	Posterior
σ_8	$\mathcal{U}(0, 2)$	$0.90^{+0.20}_{-0.18}$
$\Omega_{\rm m}$	$\mathcal{U}(0.10, 0.90)$	$0.54^{+0.26}_{-0.27}$
S_8	–	$1.16^{+0.40}_{-0.36}$
$\mu_{\rm max,true}$	$\mathcal{U}(-2, 4)$	$1.17^{+0.16}_{-0.15}$
$N_{\rm true}$	$\mathcal{U}(0, 10^4)$	3641^{+63}_{-60}

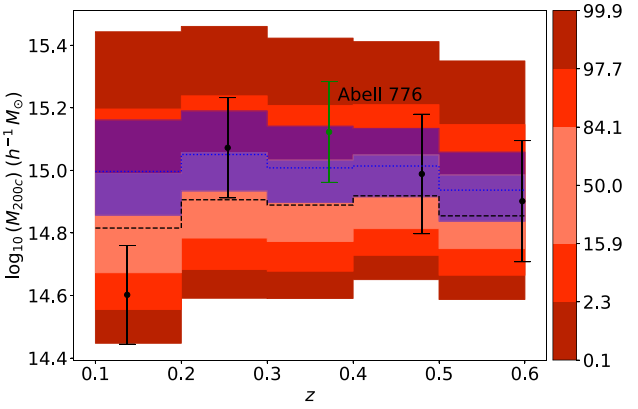

Figure 3. EVS predictions in mass-redshift space for a ΛCDM cosmology having cosmological parameters fixed to the Planck Collaboration VI (2020b) results (red contours for each redshift bin $\Delta z = 0.1$), compared with the observed largest cluster mass values from the AMICO KiDS-DR3 catalogue (black points). The green point is Abell 776's mass measurement. We also show the [16th, 84th] confidence interval predictions for a cosmology based on the maximum likelihood parameters associated to equation (11).

4.1 Compatibility of AMICO KiDS-DR3 clusters with ΛCDM predictions

We verified whether the mass measurements of AMICO KiDS-DR3 clusters are compatible with the theoretical predictions from a ΛCDM cosmology having all the cosmological parameters fixed to the Planck Collaboration VI (2020b) results.

We evaluated equations (7)–(9) in redshift bins of width $\Delta z = 0.1$, obtaining confidence intervals for the most massive galaxy cluster mass expected by the cosmological model, given by the equation:

$$\Phi(M, z) = \text{cost.}\,, \quad (12)$$

where the constant is equal to a certain quantile.

In Fig. 3, we show with red contours the predictions for the largest cluster mass value for each redshift bin, and we compare them with the observed most massive cluster mass in each bin (black points). The observed Abell 776 mass (green point) is compatible with a ΛCDM cosmology having the cosmological parameters fixed to the results from Planck Collaboration VI (2020b) within 1σ.

5 RESULTS

We constrained the posterior with a Monte Carlo Markov Chain (MCMC) analysis. As sampler, we used EMCEE (Foreman-Mackey et al. 2013), with 32 walkers and running a chain of 1000 steps, equal to ∼27 times the autocorrelation time of the chain, starting with initial positions for the walkers extracted from a Gaussian distribution centred around $\sigma_8 = 0.810$ and $\Omega_{\rm m} = 0.311$ based on Planck Collaboration VI (2020b) results, $\mu_{\rm max,true} = 1.12$ and $N_{\rm true} = 3644$

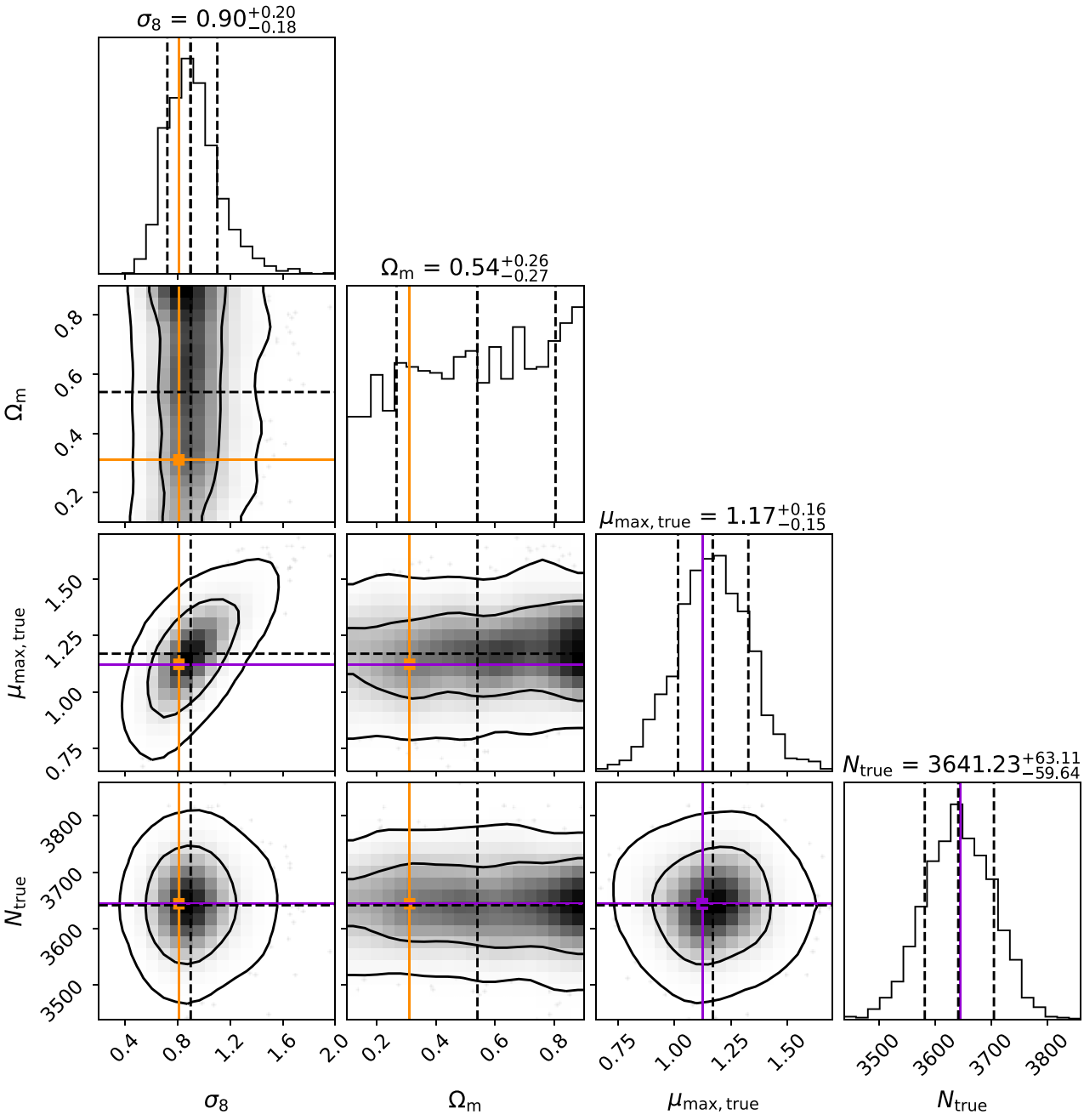

Figure 4. Corner plot showing the 16th, 50th, and 84th percentiles of the 1D parameter distributions with the 68.3 per cent and 95.4 per cent confidence regions for the corresponding 2D histograms, obtained by sampling the posterior probability distribution. Our results are shown with dashed black lines. The Planck Collaboration VI (2020b) results and the observed values $\mu_{max,obs}$ and N_{obs} are shown in orange and violet, respectively.

based on the values of $\mu_{max,obs}$ and N_{obs}. To minimize any possible influence from the starting position on the final results, we discarded the first 100 steps. We also thinned the sample with a step equal to 0.5 times the autocorrelation time. To further check for convergence, we verified that the results do not change for shorter chains.

We obtained $\sigma_8 = 0.90^{+0.20}_{-0.18}$ and $\Omega_m = 0.54^{+0.26}_{-0.27}$, as reported in Table 2. The posterior is shown in Fig. 4. While the results on σ_8 are encouraging, showing good constraints on the parameter, we are unable to provide meaningful constraints on Ω_m.

We also considered the constraints on $S_8 \equiv \sigma_8\sqrt{\Omega_m/0.3}$. The resulting distribution is shown in Fig. 6. We found $S_8 = 1.16^{+0.40}_{-0.36}$, also shown in Table 2.

6 DISCUSSION

Given the quite large statistical uncertainty, our results cannot distinguish σ_8 values as estimated either from late or early-time experiments. They are in agreement within 1σ with Planck results (Planck Collaboration VI 2020b, table 2, TT, TE, and EE+lowE). Our constraints are also in agreement within 1σ with previous results from cluster cosmology exploiting AMICO KiDS-DR3, for example the cluster counts/weak lensing joint analysis (Lesci et al. 2022b), the two-point correlation function (Lesci et al. 2022c) and the mass-bias relation (Ingoglia et al. 2022). Fig. 5 shows a comparison between our measurement and these results.

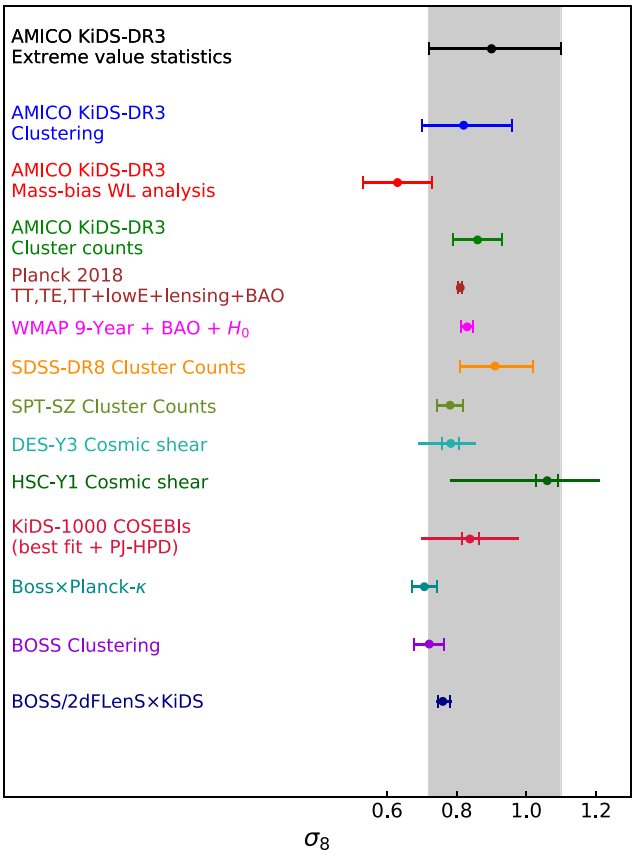

Figure 5. Comparison between σ_8 measurements obtained, from top to bottom, by using the posterior distribution derived from the likelihood of observing the most massive cluster in the AMICO KiDS-DR3 catalogue (black dot), from the analysis of the 2PCF on AMICO KiDS-DR3 catalogue presented in Lesci et al. (2022c), from the fitting of the mass-bias relation performed in Ingoglia et al. (2022), from the cluster counts/weak lensing joint analysis presented in Lesci et al. (2022b) and from the results presented in Planck Collaboration VI (2020b), Hinshaw et al. (2013), Costanzi et al. (2019), Bocquet et al. (2019), Amon et al. (2022), Secco et al. (2022), Hikage et al. (2019), Asgari et al. (2021), Chen et al. (2022), Ivanov, Simonović & Zaldarriaga (2020), and Heymans et al. (2021). The interval between the 16th and 84th percentile in our measurement is also shown in grey. The error lines associated to cosmic shear measurements are drawn with respect to the reported marginalized results, while the error caps are obtained by taking the respective constraints on S_8 and considering Ω_m fixed to the Planck Collaboration VI (2020b) result.

The relative uncertainty of our σ_8 measurement is 0.21. In comparison, the uncertainties for the Lesci et al. (2022b) cluster count and Lesci et al. (2022c) clustering results, both derived from the AMICO KiDS-DR3 catalogue, are 0.08 and 0.16, respectively. Although the EVS approach is not yet competitive with cluster count methods, its relative uncertainty is approaching that of clustering.

Ω_m is poorly constrained by the cluster mass EVS. This may be due to the fact that the order statistics with respect to mass is more sensitive to variations of σ_8 rather than of Ω_m, as verified also by Waizmann et al. (2013).

The constraint on S_8 is also in agreement within 1σ with Planck Collaboration VI (2020b) results and with previous results from cluster cosmology exploiting AMICO KiDS-DR3, for example the cluster counts/weak lensing joint analysis (Lesci et al. 2022b) and the two-point correlation function (Lesci et al. 2022c), and within 2σ from the mass-bias relation analysis (Ingoglia et al. 2022). Differently

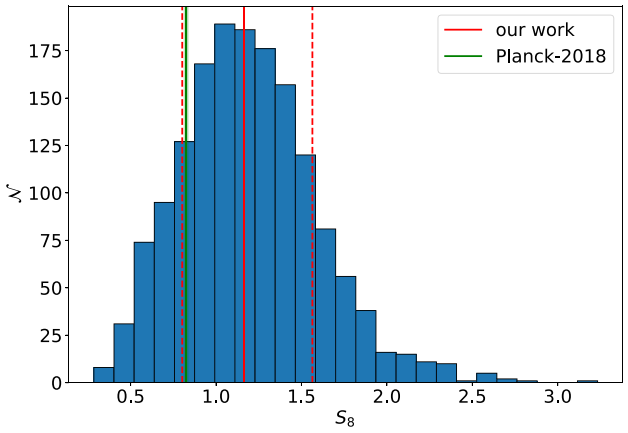

Figure 6. Sampled posterior distribution of S_8. Dashed vertical red lines show the 16th and 84th percentiles of the distribution around the median (full red line), while the green shadowed region shows the Planck Collaboration VI (2020b) result.

from other probes based on cluster cosmology, EVS is more sensitive to σ_8 rather than S_8.

We show in Fig. 3 the predictions for the [16th, 84th] confidence interval associated to the most massive cluster mass, evaluated by considering the maximum likelihood cosmological parameters obtained from equation (11). The higher σ_8 and Ω_m values with respect to the Planck Collaboration VI (2020b) results have the effect of shifting the predictions towards higher mass values.

The results reported in Section 5 have been obtained based on a relatively small sample of clusters. Considering that the EVS distribution has a variance which decreases with an increasing number of sample objects, we expect an improvement on the estimates of the cosmological parameters by using a larger catalogue.

To illustrate the effects of increasing the number of observed objects on the cosmological parameters' uncertainty, we repeated the analysis after modifying the likelihood, multiplying the number of observed clusters in the catalogue and the covered area of the sky by a factor of two. The new lower and upper uncertainties on σ_8 obtained are 0.15 and 0.20, respectively.

We then repeated the same procedure by increasing the covered sky area to 10^4 deg^2, as at the reach of Stage-IV surveys (Laureijs et al. 2011; Ivezić et al. 2019), and increasing N_{obs} by a proportional amount. This yielded lower and upper uncertainties for σ_8 equal to 0.11 and 0.15, respectively. This result shows a promising constraining power of EVS when applied to next-gen wide-field surveys, such as those proposed by ESA with *Euclid* (Euclid Collaboration 2022).

Another important element to consider is the uncertainty on the observed cluster mass, which enters the likelihood both directly, through the first factor in equation (11), and indirectly through the scale of the selection function. To determine the effects of reducing the observed cluster mass uncertainty, we repeated the analysis by considering an uncertainty of ∼20 per cent for Abell 776's mass. We obtained a new uncertainty on σ_8 equal to 0.13, which is comparable to the uncertainty obtained by increasing the covered sky area to 10^4 deg^2. This shows that a reduction of the observed mass uncertainty is another possible way to enhance the constraining power of EVS.

7 SYSTEMATIC ERRORS

Some major sources of systematic uncertainties are discussed in the following.

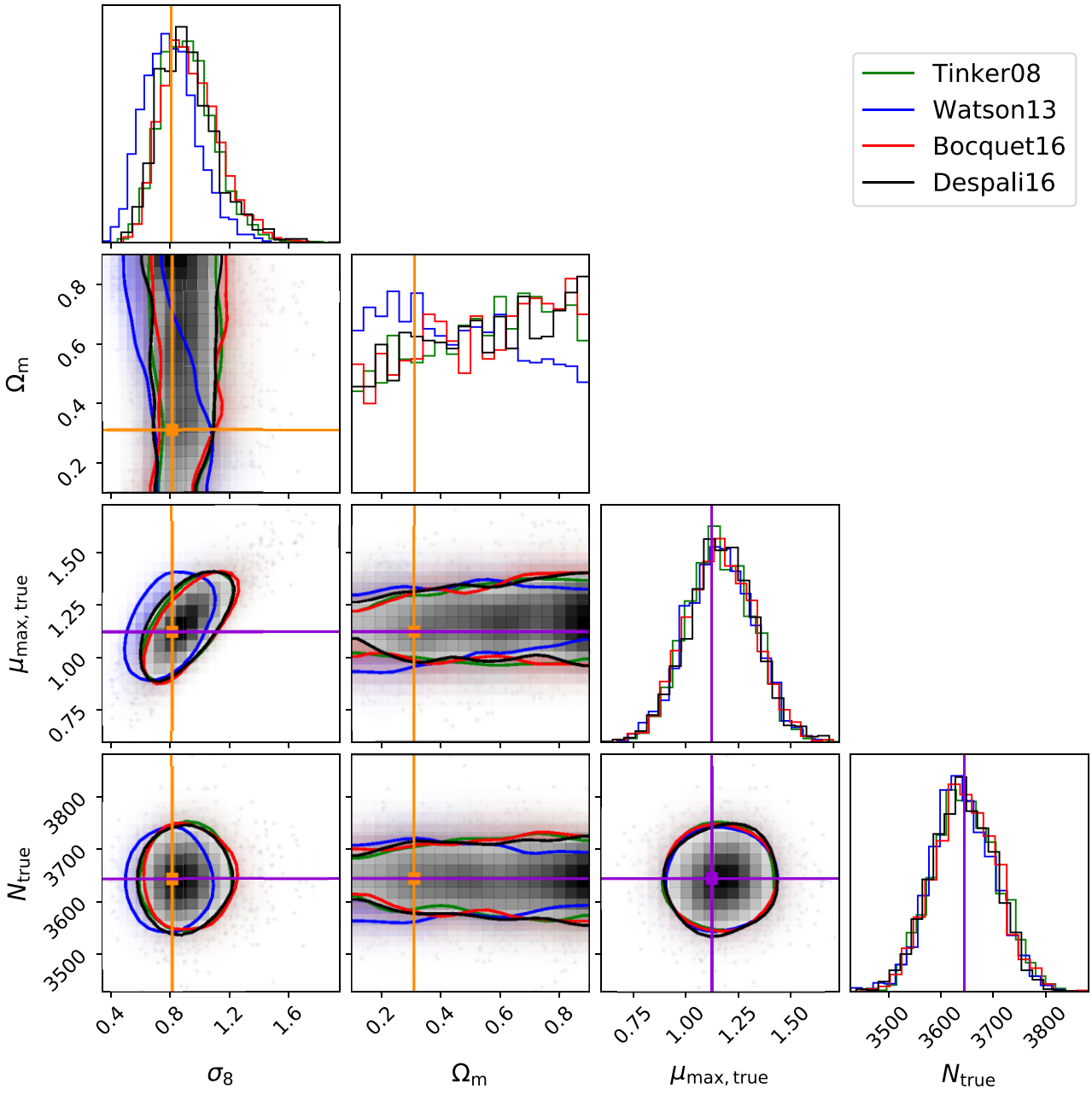

Figure 7. Same as Fig. 4, but showing also the results obtained using different halo mass functions: Tinker et al. (2008; green), Watson et al. (2013; blue), Bocquet et al. (2016; red), and Despali et al. (2016; black). The Planck Collaboration VI (2020b) results and the observed values $\mu_{max,obs}$ and N_{obs} are shown in orange and violet, respectively.

7.1 Halo mass function model

A major source of systematic uncertainty is the modelling of the halo mass function. This uncertainty, mostly due to the variation of the high-mass tail of the mass function, was estimated by repeating the MCMC analysis with three different mass function definitions other than the Despali et al. (2016) mass function.

The mass functions considered were taken from Tinker et al. (2008), Watson et al. (2013), and Bocquet et al. (2016). The corner plot showing the comparison between the four results is shown in Fig. 7, while the corresponding cosmological parameter estimates are reported in Table 3.

Table 3. Comparison between the cosmological parameter estimated with the halo mass function described in Tinker et al. (2008), Watson et al. (2013), Bocquet et al. (2016), and Despali et al. (2016), respectively.

HMF definition	σ_8	Ω_m	S_8
Tinker-2008	$0.91^{+0.19}_{-0.17}$	$0.55^{+0.23}_{-0.29}$	$1.19^{+0.37}_{-0.36}$
Watson-2013	$0.79^{+0.19}_{-0.17}$	$0.46^{+0.28}_{-0.24}$	$0.95^{+0.22}_{-0.23}$
Bocquet-2016	$0.92^{+0.21}_{-0.17}$	$0.56^{+0.24}_{-0.29}$	$1.22^{+0.43}_{-0.40}$
Despali-2016	$0.90^{+0.20}_{-0.18}$	$0.54^{+0.26}_{-0.27}$	$1.16^{+0.40}_{-0.36}$

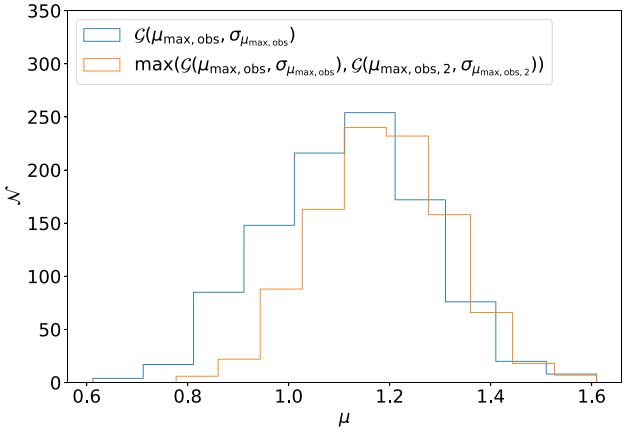

Figure 8. Comparison between the distribution associated to Abell 776's mass measurement, $\mathcal{G}(\mu_{\max,\,\mathrm{obs}}, \sigma_{\mu_{\max,\,\mathrm{obs}}})$, and the distribution $\max[\mathcal{G}(\mu_{\max,\,\mathrm{obs}}, \sigma_{\mu_{\max,\,\mathrm{obs}}}),\ \mathcal{G}(\mu_{\max,\,\mathrm{obs},\,2}, \sigma_{\mu_{\max,\,\mathrm{obs},\,2}})]$.

The difference between the highest and the lowest obtained central values for the parameters σ_8, Ω_m, and S_8 is $(\Delta\sigma_8)_\mathrm{HMF} = 0.13$, $(\Delta\Omega_\mathrm{m})_\mathrm{HMF} = 0.10$, and $(\Delta S_8)_\mathrm{HMF} = 0.27$. These values can be taken as estimates of the systematic error due to the uncertainty on the halo mass function model assumption.

7.2 Mass ranking

A potential source of uncertainty is the misidentification of the most massive cluster. We considered Abell 776 as the most massive cluster of the catalogue. Due to scatter and observational uncertainties, this might not be the case.

According to the WL mass calibration we adopted, the second most massive cluster of the catalogue, J140101.92+025218, is located at redshift $z = 0.25$ and has a mass equal to $M_{\max,\,\mathrm{obs},\,2} = (11.8 \pm 4.4) \times 10^{14}\,h^{-1}\,\mathrm{M}_\odot$, which is comparable to the observed mass value of Abell 776, $M_{\max,\,\mathrm{obs}} = (13.3 \pm 4.9) \times 10^{14}\,h^{-1}\,\mathrm{M}_\odot$, and could thus be a candidate as the true most massive galaxy cluster of the sample. There could then be a systematic error contribution due to having underestimated the true value of the biggest mass measurement of the catalogue.

To evaluate this contribution, we extracted $N = 1000$ random samples from two Gaussian distributions, $\mathcal{G}(\mu_{\max,\,\mathrm{obs}}, \sigma_{\mu_{\max,\,\mathrm{obs}}})$ and $\mathcal{G}(\mu_{\max,\,\mathrm{obs},\,2}, \sigma_{\mu_{\max,\,\mathrm{obs},\,2}})$, associated to the first and second observed most massive cluster of the sample, respectively, and having a standard deviation given by the corresponding mass measurement uncertainty. We then constructed a new distribution by comparing term-wise the extracted samples and choosing the maximum between the two values. This corresponds to the distribution of $\max[\mathcal{G}(\mu_{\max,\,\mathrm{obs}}, \sigma_{\mu_{\max,\,\mathrm{obs}}}),\ \mathcal{G}(\mu_{\max,\,\mathrm{obs},\,2}, \sigma_{\mu_{\max,\,\mathrm{obs},\,2}})]$.

We compared the mean of this new distribution to Abell 776's mass, obtaining a difference between the two of $\delta M = 0.07$, which is lower than the statistical uncertainty on the cluster masses. The comparison between the two distributions is shown in Fig. 8. We can consider this systematic error to have a negligible effect on the results.

7.3 Reference cosmological parameters

In the procedure detailed in Section 4, we considered all the cosmological parameters other than Ω_m and σ_8 fixed to the values from Planck Collaboration VI (2020b). To determine how much the results are robust with respect to a variation in these parameters, we repeated the analysis by letting one more parameter, the spectral index, vary. The results are shown in Fig. 9, and the corresponding parameter estimates are reported in Table 4.

A degeneracy in the n_s–σ_8 plane can be seen. Indeed, the Spearman linear correlation index between n_s and σ_8, defined as the ratio between the covariance of the ranks associated to n_s and σ_8 samples, $\mathrm{cov}(R(n_\mathrm{s}), R(\sigma_8))$, and the product of the respective rank uncertainties, $\sigma_{R(n_\mathrm{s})} \cdot \sigma_{R(\sigma_8)}$, is $\rho_\mathrm{s} = 0.61$, with an associated p-value of $\gtrsim 0$.

The results shown in Table 4 are consistent with the Planck Collaboration VI (2020b) results. The 84th percentile associated to σ_8 increased by 55 per cent with respect to the value in Table 2, while the 16th percentile increased by 39 per cent. The spectral index n_s could not be significantly constrained.

8 CONCLUSIONS

In this work, we estimated σ_8 using the EVS applied to galaxy clusters (Waizmann et al. 2013), by considering the probability of observing the most massive cluster of the AMICO KiDS-DR3 catalogue (Maturi et al. 2019). By excluding all clusters outside the redshift interval $z \in [0.10, 0.60]$ and with an intrinsic richness $\lambda^* \leq 20$, the sample consists of $N_\mathrm{obs} = 3644$ clusters, observed in an effective region of the sky equal to $377\,\mathrm{deg}^2$. Our analysis accounted for the uncertainties associated to the largest cluster mass measurement and total cluster count measurement, respectively.

We obtained $\sigma_8 = 0.90^{+0.20}_{-0.18}$. The result is compatible with the constraints obtained by Planck Collaboration VI (2020b) and previous AMICO KiDS-DR3 results (Ingoglia et al. 2022; Lesci et al. 2022b, c) within 1σ. Constraints on Ω_m are not significant. This is caused by the fact that the mass EVS is most sensitive to σ_8, rather than Ω_m.

We also determined $S_8 = 1.16^{+0.40}_{-0.36}$. This result, while being quite prior-dependent, is compatible within 1σ with measurements from Planck Collaboration VI (2020b) and Lesci et al. (2022b, c) and within 2σ with results from Ingoglia et al. (2022).

The main source of systematic error comes from the uncertainty on the halo mass function model: by repeating the analysis with three other halo mass functions, (Tinker et al. 2008; Watson et al. 2013; Bocquet et al. 2016), we obtained an estimate of the systematic uncertainty by considering the difference between the highest and lowest central value for each parameter of interest. These uncertainties are equal to $(\Delta\sigma)_\mathrm{HMF} = 0.13$, $(\Delta\Omega_\mathrm{m})_\mathrm{HMF} = 0.10$, and $(\Delta S_8)_\mathrm{HMF} = 0.27$, which are much lower than the respective statistical uncertainty contributions. The systematic uncertainties due to the uncertainty on the cluster mass ordering and due to having fixed all the other cosmological parameters are, instead, all negligible.

EVS of cluster masses is highly complementary to number count analyses. It is mostly sensitive to σ_8 rather than S_8, and joint analyses could break degeneracies between σ_8 and Ω_m. Differently from number count analyses, selection function effects, purity and completeness play a small role in EVS. On the other hand, EVS is strongly affected by the theoretical uncertainty on the exponential tail of the halo mass function.

Our results have been obtained on a relatively small sample of galaxy clusters, located in a relatively small fraction of the sky. To test the effects of a larger catalogue, we doubled the number of observed clusters, obtaining lower and upper uncertainties on σ_8 of 0.15 and 0.20, respectively. By increasing the covered sky area to $10^4\,\mathrm{deg}^2$, as at the reach of Stage-IV surveys (Laureijs et al. 2011; Ivezić et al. 2019), we instead obtained lower and upper uncertainties on σ_8 of 0.11 and 0.15.

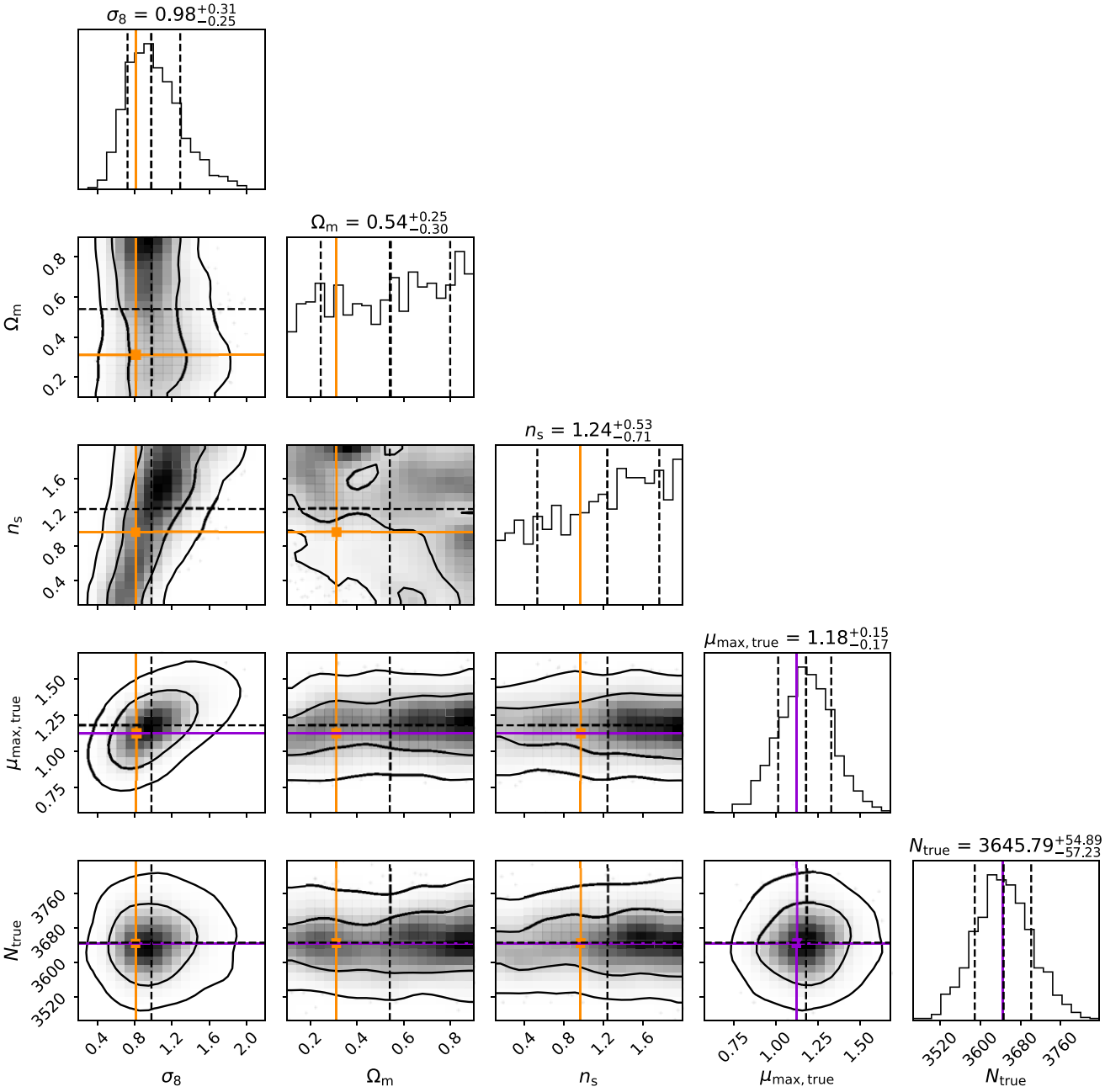

Figure 9. Corner plot showing the 16th, 50th, and 84th percentiles of the 1D parameter distributions with the 68.3 per cent and 95.4 per cent confidence regions for the corresponding 2D histograms, obtained by sampling the posterior probability distribution, considering the spectral index n_s as a free parameter. Our results are shown with dashed black lines. The Planck Collaboration VI (2020b) results and the observed values $\mu_{max,obs}$ and N_{obs} are shown in orange and violet, respectively.

Table 4. Parameters associated to the likelihood distribution described in Section 4, estimated by considering the spectral index as a free parameter.

Parameter	Prior	Posterior
σ_8	$\mathcal{U}(0, 2)$	$0.98^{+0.31}_{-0.25}$
Ω_m	$\mathcal{U}(0.10, 0.90)$	$0.54^{+0.25}_{-0.30}$
S_8	–	$1.26^{+0.47}_{-0.41}$
n_s	$\mathcal{U}(0.1, 2)$	$1.24^{+0.53}_{-0.71}$
$\mu_{max,true}$	$\mathcal{U}(-2, 4)$	$1.18^{+0.15}_{-0.17}$
N_{true}	$\mathcal{U}(0, 10^4)$	3646^{+55}_{-57}

Another route to obtain tighter constraints is to reduce the uncertainty on the cluster mass estimates. By halving the uncertainty on the mass estimate (i.e. considering a mass uncertainty of ∼20 per cent), we indeed obtain an uncertainty on σ_8 of 0.13, comparable to the reduction obtained due to increasing the covered sky area by 27 times its original value.

We plan to extend this analysis to the latest KiDS data release (DR5; Wright et al., in preparation), as well as DR4 (Kuijken et al. 2019), which covers an area of the sky of $\sim 10^3$ deg^2 (almost 2.5 times larger than the one associated to the DR3), and *Euclid* Data Release 1. An even more powerful application of our technique will indeed be possible with observations from the *Euclid* Space Telescope (Laureijs

et al. 2011) or the Vera C. Rubin Observatory (Ivezić et al. 2019), which are expected to detect thousands of distant massive clusters (see e.g. Sartoris et al. 2016). Future surveys will also detect high mass clusters at very large redshifts ($z \gtrsim 1$), where the leverage of EVS can be very effective. Future works on this topic will also focus on understanding the potential of considering more than one cluster mass simultaneously to obtain the parameter constraints, as well as checking if there is any upper limit on the number of simultaneous clusters that one can consider for the joint constraints. We will also check under which conditions specifically the EVS approach is more competitive than other methods, e.g. cluster count or clustering.

ACKNOWLEDGEMENTS

Based on data products from observations made with ESO Telescopes at the La Silla Paranal Observatory under programme IDs 177.A-3016, 177.A3017 and 177.A-3018, and on data products produced by Target/OmegaCEN, INAF-OACN, INAF-OAPD and the KiDS production team, on behalf of the KiDS consortium. MS acknowledges financial contributions from contract ASI-INAF n.2017-14-H.0 and contract INAF mainstream project 1.05.01.86.10. LM acknowledges support from the grants PRIN-MIUR 2017 WSCC32 and ASI n.2018-23-HH.0. MR acknowledges support from the INAF mini-grant 2022 "GALCLOCK". All the cosmological functions used for the statistical analysis are built using the PYTHON cosmology library COLOSSUS[2] (Diemer 2018), while the MCMC analysis has been performed with the PYTHON library EMCEE[3] (Foreman-Mackey et al. 2013) and the resulting corner plots have been drawn using the PYTHON library CORNER.PY[4] (Foreman-Mackey 2016). We thank Konrad Kuijken for constructive criticism of the paper. We thank the anonymous referee for his comments, which helped us to better present our results.

DATA AVAILABILITY

The data underlying this article will be shared on reasonable request to the corresponding author. The AMICO KiDS-DR3 cluster catalogue is publicly available and can be accessed via the VizieR Online Data Catalogue (Lesci et al. 2022a).

REFERENCES

Abdalla E. et al., 2022, J. High Energy Astrophys., 34, 49
Amon A. et al., 2022, Phys. Rev. D, 105, 023514
Asgari M. et al., 2021, A&A, 645, A104
Bellagamba F., Maturi M., Hamana T., Meneghetti M., Miyazaki S., Moscardini L., 2011, MNRAS, 413, 1145
Bellagamba F., Roncarelli M., Maturi M., Moscardini L., 2018, MNRAS, 473, 5221
Bellagamba F. et al., 2019, MNRAS, 484, 1598
Bhavsar S. P., Barrow J. D., 1985, MNRAS, 213, 857
Bocquet S., Saro A., Dolag K., Mohr J. J., 2016, MNRAS, 456, 2361
Bocquet S. et al., 2019, ApJ, 878, 55
Capaccioli M., Schipani P., 2011, The Messenger, 146, 2
Chen S.-F., White M., DeRose J., Kokron N., 2022, J. Cosmol. Astropart. Phys., 2022, 041
Corasaniti P.-S., Sereno M., Ettori S., 2021, ApJ, 911, 82
Costanzi M. et al., 2019, MNRAS, 488, 4779
Davis O., Devriendt J., Colombi S., Silk J., Pichon C., 2011, MNRAS, 413, 2087
de Jong J. T. A. et al., 2013, The Messenger, 154, 44
de Jong J. T. A. et al., 2015, A&A, 582, A62
de Jong J. T. A. et al., 2017, A&A, 604, A134
Despali G., Giocoli C., Angulo R. E., Tormen G., Sheth R. K., Baso G., Moscardini L., 2016, MNRAS, 456, 2486
Diemer B., 2018, ApJS, 239, 35
Douspis M., Salvati L., Aghanim N., 2019, preprint (arXiv:1901.05289)
Euclid Collaboration, 2022, A&A, 662, A112
Foreman-Mackey D., 2016, J. Open Source Softw., 1, 24
Foreman-Mackey D., Hogg D. W., Lang D., Goodman J., 2013, PASP, 125, 306
Gumbel E. J., 1958, Statistics of Extremes. Columbia Univ. Press, New York Chichester
Hamana T., Shirasaki M., Lin Y.-T., 2020, PASJ, 72, 78
Harrison I., Coles P., 2011, MNRAS, 421, L19
Heymans C. et al., 2021, A&A, 646, A140
Hikage C. et al., 2019, PASJ, 71, 43
Hinshaw G. et al., 2013, ApJS, 208, 19
Holz D. E., Perlmutter S., 2012, ApJ, 755, L36
Ingoglia L. et al., 2022, MNRAS, 511, 1484
Ivanov M. M., Simonović M., Zaldarriaga M., 2020, J. Cosmol. Astropart. Phys., 2020, 042
Ivezić Ž. et al., 2019, ApJ, 873, 111
Kim J. et al., 2021, ApJ, 923, 101
Kuijken K., 2011, The Messenger, 146, 8
Kuijken K. et al., 2015, MNRAS, 454, 3500
Kuijken K. et al., 2019, A&A, 625, A2
Laureijs R. et al., 2011, preprint (arXiv:1110.3193)
Lesci G. F. et al., 2022a, VizieR Online Data Catalogue, 665, 100
Lesci G. F. et al., 2022b, A&A, 659, A88
Lesci G. F. et al., 2022c, A&A, 665, A100
Lovell C. C., Harrison I., Harikane Y., Tacchella S., Wilkins S. M., 2022, MNRAS, 518, 2511
Maturi M., Meneghetti M., Bartelmann M., Dolag K., Moscardini L., 2005, A&A, 442, 851
Maturi M., Bellagamba F., Radovich M., Roncarelli M., Sereno M., Moscardini L., Bardelli S., Puddu E., 2019, MNRAS, 485, 498
Medezinski E. et al., 2018, PASJ, 70, S28
Navarro J. F., Frenk C. S., White S. D. M., 1997, ApJ, 490, 493
Planck Collaboration I, 2014, A&A, 571, A1
Planck Collaboration XXVII, 2016, A&A, 594, A27
Planck Collaboration I, 2020a, A&A, 641, A1
Planck Collaboration VI, 2020b, A&A, 641, A6
Pratt J., Baraffe I., Goffrey T., Constantino T., Viallet M., Popov M. V., Walder R., Folini D., 2017, A&A, 604, A125
Radovich M. et al., 2017, A&A, 598, A107
Reischke R., Maturi M., Bartelmann M., 2016, MNRAS, 456, 641
Sartoris B. et al., 2016, MNRAS, 459, 1764
Schechter P., 1976, ApJ, 203, 297
Secco L. F. et al., 2022, Phys. Rev. D, 105, 023515
Sereno M., 2015, MNRAS, 450, 3665
Sereno M., Ettori S., 2015, MNRAS, 450, 3675
Sereno M. et al., 2020, MNRAS, 497, 894
Sheth R. K., Diaferio A., 2011, MNRAS, 417, 2938
Tinker J., Kravtsov A. V., Klypin A., Abazajian K., Warren M., Yepes G., Gottlöber S., Holz D. E., 2008, ApJ, 688, 709
Waizmann J. C., Ettori S., Moscardini L., 2011, MNRAS, 418, 456
Waizmann J. C., Ettori S., Moscardini L., 2012, MNRAS, 420, 1754
Waizmann J.-C., Ettori S., Bartelmann M., 2013, MNRAS, 432, 914
Watson W. A., Iliev I. T., D'Aloisio A., Knebe A., Shapiro P. R., Yepes G., 2013, MNRAS, 433, 1230

[2] https://bdiemer.bitbucket.io/colossus/index.html
[3] https://emcee.readthedocs.io/en/stable/
[4] https://corner.readthedocs.io/en/stable/

This paper has been typeset from a TEX/LATEX file prepared by the author.